1DH MODEL PREDICTS TRANSPORT AND SEDIMENTATION INSIDE A HOPPER

The model performs well even though several physical simplifications have been made.

Trailing Suction Hopper Dredgers (TSHDs) are commonly used in the dredging industry for a wide variety of maintenance, land reclamation and maritime construction projects. During trailing suction dredging, the TSHD trails drag heads over the seabed to excavate it. Loosened bed materials like sand, clay or gravel together with surrounding water are hydraulically sucked up by pumps through the trailing suction pipes and this mixture is subsequently discharged into the ship's cargo hold called a hopper.

Accurately quantify sediment in a hopper

A novel transient one-dimensional horizontal simulation model that predicts the multi-fractional transport and sedimentation of sand along a hopper of a Trailing Suction Hopper Dredger (TSHD) has been developed. The model includes an external current model and an internal current model mutually coupled by vertical exchange processes. It solves cross-section averaged mass and momentum equations to predict sediment transport by barotropic and baroclinic currents. Relevant vertical physical processes are modelled using closure relations for hindered settling, entrainment, erosion and *continuity-based* vertical transport of water and sediment. Deposition and erosion closures dynamically couple both the external current model and the internal current model with a sediment bed model.

A practical simulation tool is provided which balances the need of sufficient predictive capability through simulation of time and along hopper variation of model quantities with the requirement of low computational effort and complexity compared to transient two-dimensional vertical or three-dimensional models through the use of closure assumptions to model vertical processes. The model verification against a number of analytical solutions for idealised test cases indicates that the discretised model is mass, momentum and mechanical energy conservative. Moreover, it demonstrates that the model can cope with drying and flooding phenomena and with transitions from subcritical flow to supercritical flow and vice versa. The model validation against laboratory and prototype measurements shows that our model predicts the total cumulative overflow losses for a wide range of conditions on laboratory and prototype scale well at low user complexity level and at low computational time.

Introduction

Upon entering a Trailing Suction Hopper Dredger's hopper, suspended sediment disperses and settles throughout the volume to form a sediment bed layer at the bottom. Once the water level inside the hopper exceeds the overflow level, surplus water in the hopper flows through the overflow and back into the water surrounding the vessel. The overflowing water can contain sediment particles which remain in suspension. Hence, part of the sediment placed into the hopper is discharged to the surrounding water and consequently the loading production is lower than the suction production. Therefore, the simulation of sedimentation processes in hoppers is of great interest to provide predictions of how efficiently the incoming sediment is retained in the hopper.

Downfalls of past approaches

Several mathematical approaches exist to model the sedimentation process taking place within the hopper of TSHDs. Though, it was developed for the design of sewage and water treatment tanks Camp's equilibrium point model can be considered to be one of the first (Camp, 1946). His modelling framework has been the basis for the development of several other point models with more physical realism. For example, Groot (1981) added the effects of hindered settling to Camp's model. Vlasblom & Miedema (1995) and Miedema & Vlasblom (1996) simplified Camp's equations and included bed level changes due to (hindered) settling and erosion as well as the effect of varying overflow levels. Ooijens (1999) extended Vlasblom & Miedema's (1995) model to include unsteady effects so that the previous states can influence the current state.

Although the aforementioned models can provide reasonable overflow loss predictions after calibration, they lack predictive capability as this model approach does not simulate processes such as erosion and sedimentation on a more local time and spatial scale. Therefore, other researchers have developed more process-based transient one-dimensional vertical (1DV) Reynolds Averaged Navier Stokes (RANS) (van Rhee, 2002; Spearman, 2014) and two-dimensional vertical (2DV RANS) models (van Rhee, 2002). These models include transient flow, transport, mixing and settling variation in the vertical (1DV & 2DV) and in the horizontal (2DV). With the 2DV modelling approach van

Rhee (2002) showed the importance of gravity currents for the transport, sedimentation and bed level development along the hopper and overflow loss predictions.

In general, previous models have a number of shortcomings that favour the development of a new model:

- except for 2DV models, they do not include transport variation in the horizontal by gravity currents which would make their use inappropriate to predict the along hopper sediment bed layer distribution,
- previous models cannot deal with drying and flooding of the sediment bed, for instance when removing the excess water with the overflow or when loading coarse material,
- previous models do not include the option to vary the hopper cross-section with the depth and height of the current, and
- they include very simple inflow and overflow conditions.

This article describes the development of a new process-based transient one-dimensional horizontal (1DH) simulation model with cross-section averaged variables. It includes the most relevant physics to provide sound physical predictions of the overflow losses and longitudinal distribution of the hopper sediment bed layer, but with low computational effort and low user complexity. To achieve this, a less elaborate system of equations is solved as 2DV and 3D models by using closure relationships to model vertical exchange processes. This approach hence omits the simulation of these processes and of vertical variations as there is inherent uncertainty (de Nijs, 2010) in favour of having model simulation predictive capability along the hopper of transport and sedimentation from currents caused by baroclinic and barotropic pressure gradients in contrast to 1DV RANS models.

Governing transport and sedimentation equations

Model approach

In a hopper, there is horizontal through flow from the inflow position to overflow position due to incoming water, which sets up a barotropic pressure gradient. The barotropic pressure gradient is caused by the water level gradient and it does not depend on the position within the water column (see Figure 1).

At the inflow position, the inflowing mixture of relatively high density propagates as vertical buoyant jets towards the hopper bottom/sediment bed. Here they deflect and subsequently evolve into horizontally propagating sediment-laden gravity currents that remain near the bed along the hopper (de Koning, 1977, van Rhee, 2002). These gravity currents dominate the along hopper transport of suspended sediment and sediment bed formation (van Rhee, 2002). Baroclinic pressure gradients and bed slopes generate the horizontal gravity currents. Surfaces of constant density that are not parallel to surfaces of constant pressure cause the baroclinic pressure gradients which depend on the position within the water column (see Figure 2 and de Nijs et al., 2011).

In our model approach, a water layer of approximately homogeneous density is distinguished, that is negligible density differences overlaying a gravity current with small height relative to the total water depth. Hydrostatic pressure distributions are assumed because the ratio depth water layer overlaying the gravity current to hopper length is much smaller than one. Furthermore, it is assumed the gravity current does not affect the overlaying water layer because the ratio gravity current height to water depth is smaller than one (de Nijs, 2010). These assumptions allow us to model the current of the overlaying water layer without baroclinic effects caused by the gravity current near the bed. Hereafter, this part of the modelling is referred to as the external current model. The gravity current near the bed is modelled with gravity current cross-section averaged conservation equations for mass and momentum similar to de Nijs (2010). Taken into account is the water layer overlaying the gravity current influences the gravity current. That is, the gravity current is not only forced by relative density differences and bed level gradients, but also by the slope of the water level in the hopper (see Figure 2). Hereafter, this part of the modelling is referred to as the internal current model.

The external and internal current models calculate horizontal multi-fractional transport of suspended sediment inside the hopper within a transient one-dimensional horizontal cross-section averaged mathematical framework. This framework enables the user to specify hopper cross-section variations with depth/height of the current. The external current and internal current models are mutually coupled through vertical sediment transports (see Figure 3). These vertical sediment exchanges include upward transport by vertical hopper through flow, settling and entrainment. Both the external current and internal current models

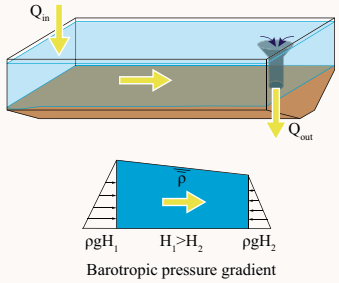

FIGURE 1

The through flow in the hopper caused by the barotropic pressure gradient.

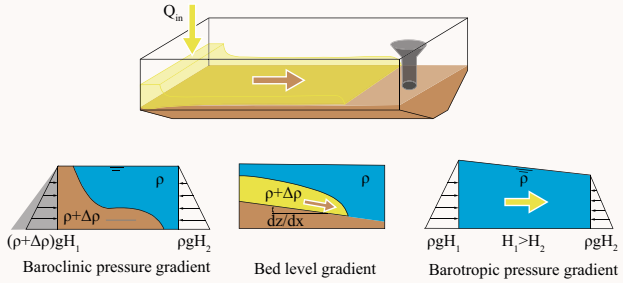

FIGURE 2

The internal current set-up by the baroclinic pressure gradient, bed level gradient and the barotropic pressure gradient, respectively.

$$\frac{\partial A_e}{\partial t}+\frac{\partial A_e U_e}{\partial x}=-\frac{\rho_b}{\rho_w}\frac{\partial A_b}{\partial t}+\left(P_{in,w,e}+P_{in,\phi,e}\right)B/\rho_w-\Delta\left(\left(P_{in,\phi,e}B+(E-D)B-P_{ov,\phi}B_{ov}\right)/\rho_s\right)-\left(P_{ov,w}+P_{ov,\phi}\right)B_{ov}/\rho_w$$

$$\frac{\partial \phi_e A_e}{\partial t}+\frac{\partial \phi_e A_e U_e}{\partial x}=\left(P_{in,\phi,e}B+(E-D_e)B+P_{E,\phi}B+P_{upw,\phi}B-P_{ov,\phi}B_{ov}\right)/\rho_s$$

$$\frac{\partial U_e A_e}{\partial t}+\frac{\partial U_e^2 A_e}{\partial x}+gA_e\frac{\partial \xi_e}{\partial x}+c_f|U_e|U_eP=0$$

$$\rho_b=(1-n_0)\rho_s+n_0\rho_w,\qquad \Delta=\left(\frac{\rho_s-\rho_w}{\rho_w}\right)$$

(2)

$$\frac{\partial A_i}{\partial t}+\frac{\partial A_i U_i}{\partial x}=-\frac{\rho_b}{\rho_w}\frac{\partial A_b}{\partial t}-\Delta\left(\left(P_{in,\phi,i}B+D_eB+(E-D_i)B-P_{E,\phi}B-P_{upw,\phi}B\right)/\rho_s\right)+\left(P_{in,\phi,i}+P_{in,w,i}\right)B/\rho_w$$

$$\frac{\partial \phi_i A_i}{\partial t}+\frac{\partial \phi_i A_i U_i}{\partial x}=\left(P_{in,\phi,i}B+D_eB+(E-D_i)B-P_{E,\phi}B-P_{upw,\phi}B\right)/\rho_s$$

$$\frac{\partial U_i A_i}{\partial t}+\frac{\partial U_i^2 A_i}{\partial x}+\frac{\partial \frac{1}{2}\varepsilon g h A_i}{\partial x}+\frac{\rho_e}{\rho_i}gA_i\frac{\partial \xi_e}{\partial x}+\varepsilon gA_i\frac{\partial z}{\partial x}=-\frac{\tau_b B_b}{\rho_i}-\frac{U}{\sqrt{U^2}}\frac{\tau_i B_i}{\rho_i}$$

$$\varepsilon=\left(\frac{\rho_i-\rho_e}{\rho_e}\right)$$

(3)

also take into account sediment exchanges with the sediment bed due to erosion and deposition.

Governing equations

The model simulates transport of water and sediment inside a hopper with cross-section averaged conservation equations of mass and momentum similar as de Nijs (2010). The equations of the external and internal current have been reformulated by substituting the conservation equation of sediments into the mass conservation equation for the mixture to derive a solvable conservative system of equations. This results in three conservation equations for the water-sediment mixture, sediment concentration for multiple sediment fractions and momentum of the external flow caused by the barotropic pressure gradient and the internal flow caused by the combination barotropic and baroclinic pressure gradients, respectively.

The bed level variation due to sediment bed exchange processes based on mass conservation is similar as Van Rhee (2002):

$$\frac{\partial A_b}{\partial t}=\frac{(D-E)B_b}{(1-n_0-\phi)}$$

(1)

Where A_b is the cross-sectional area of the sediment bed, t is time, D is the sediment deposition flux, E is the sediment erosion flux, B_b is the width of the bed interface, n_0 is the bed porosity and ϕ is the cross-section averaged concentration in the current above the bed.

The conservation equations of the external current and sediment transport read: (see 2) Where A_e is the cross-sectional area of the external current, U_e is the cross-section averaged horizontal external current velocity, B is the width of the hopper, x is a horizontal spatial distance, ϕ_e is the cross-section averaged concentration in the external current, ρ_s is the solids density of sand, ρ_w is the water density, ρ_e is the external cross-section averaged density, g is the gravitational acceleration, ξ_e is the water level inside the hopper, c_f is a dimensionless friction coefficient, P is the wetted perimeter, D_e is the sediment deposition flux of the external current, $P_{in,w}$ and $P_{in,\phi}$ are the inflowing water and sediment flux, P_E is the entrainment flux, $P_{ov,w}$ and $P_{ov,\phi}$ are the overflowing water and sediment fluxes and $P_{upw,\phi}$ is the upward sediment flux due to the upward through flow in the hopper.

The conservation equations of the internal current and sediment transport are: (see 3)

Where A_i is the cross-sectional area of the internal current, U_i is the cross-section averaged horizontal internal current velocity, ϕ_i is the cross-section averaged concentration in the internal current, h is the internal current height, B_i is the interface width between the external and internal current, ρ_i is the internal cross-section averaged density, z is the sediment bed height, D_i is the deposition flux of the internal current, τ_b is the bed shear stress and τ_i is the interfacial stress between the external and internal currents.

Closure relations

The following closure relations are defined to close the set of conservation equations. The sand-water mixture discharge into the hopper is defined at a specified location along the hopper. This mixture entering the hopper is divided into a sediment- and water discharge for respectively the external and internal current as follows:

$$P_{in,\phi,e}=\alpha\rho_s\phi_{in}\left(\frac{Q_{in}}{A_{in}}\right),\qquad P_{in,\phi,i}=(1-\alpha)\rho_s\phi_{in}\left(\frac{Q_{in}}{A_{in}}\right)$$

(4)

Where ϕ_{in} is the mixture concentration discharged into the hopper, Q_{in} is the mixture flow discharged into the hopper, A_{in} is the inflow area and α is a distribution factor to define the percentage of the incoming sediment flux which enters either the external current or the internal current. Here it is assumed that the discharged mixture flows directly towards the bottom of the hopper as a buoyant jet into the internal current so α is set 0. The water discharged into the hopper is:

$$P_{in,w,e}=\rho_w(1-\phi_{in})\left(\frac{Q_{in}}{A_{in}}\right),\qquad P_{in,w,i}=\rho_w(1-\phi_{in})\left(\frac{Q_{in}}{A_{in}}\right)$$

(5)

Note that the water flux contributes to both the external current and internal current.

The overflow can be positioned at arbitrary positions along the hopper and levels. It is noted that confidential in-house developed mathematical expressions are applied to model the overflow discharge. The overflowing mixture is also divided in a water- and sediment flux:

$$P_{ov,w}=\rho_w(1-\phi_{ov})\left(\frac{Q_{ov}}{A_{ov}}\right),\quad P_{ov,\phi}=\rho_s\phi_{ov}\left(\frac{Q_{ov}}{A_{ov}}\right)$$

(6)

Where ϕ_{ov} is the cross-section averaged concentration in the external current at the

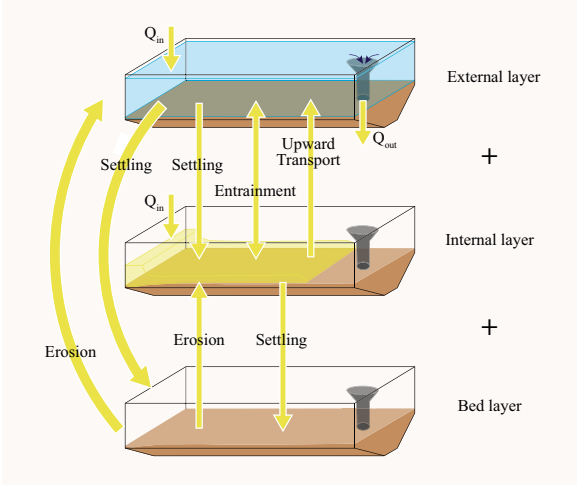

FIGURE 3

Sediment exchanges between the internal current and external current model, and between both current models and the sediment bed.

position of the overflow, Q_{ov} is the overflow discharge and A_{ov} is the cross-sectional area of the overflow. Note that the water and sediment fluxes coming into and out of the hopper are only active at specific locations along the hopper.

Sediment exchange between the sediment bed and the overlaying currents are due to deposition and erosion. The deposition flux of the external current enters the internal current first when there is an internal current, else it directly enters the sediment bed. The deposition flux of the internal current directly enters the sediment bed. The cross-sectional averaged deposition flux of the internal and external currents for multiple fractions is based on hindered settling (Richardson & Zaki, 1954) and the near bed concentration as follows:

$$D = (w_{s,k} - w)\phi_k \rho_s$$

(7)

Where ϕ_k is the cross-section averaged concentration in either the external or internal current where subscript k refers to the sediment size fraction, w is an upward velocity and $w_{s,k}$ is the hindered settling velocity of a certain fraction k (Richardson & Zaki, 1954):

$$w_{s,k} = w_{0,k}(1 - \phi_t)^{n_k} \quad with\ \phi_t = \sum_{k=1}^{N} \phi_k$$

(8)

Where $w_{0,k}$ is the settling velocity of a single grain of a certain size fraction k (Ferguson & Church, 2004), ϕ_t is the total cross-sectional averaged concentration of either the external or internal current and n_k is an empirical expression (Rowe, 1987) for a certain size fraction k.

Because of continuity constraints the inflowing water causes upward through flow in the hopper. This upward flow transports sediment from the internal current into the external current. The upward transport velocity is the upward velocity minus the settling velocity so that the upward sediment flux reads:

$$P_{upw;\phi} = (w - w_{s,k})\phi_{i,k}\rho_s$$

(9)

Where w is an upward velocity in the hopper caused by the inflowing water and continuity and $\phi_{i,k}$ is the cross-section averaged concentration of the internal current for size fraction k. The upward flow velocity is calculated from water flowing into the hopper and the horizontal hopper surface as follows:

$$w = \frac{Q_{in}}{BL}$$

(10)

Where B is the width of the hopper and L is the length of the hopper.

Sediment erosion from the bed layer into the overlaying current is described with a pick-up flux (Van Rijn, 1984) corrected with an in-house confidential erosion correction factor (R_c):

$$E = R_c \phi_p \rho_s \sqrt{g\Delta d}$$

(11)

Where ϕ_p is the dimensionless pick-up flux (Van Rijn, 1984), d is the particle diameter, Δ is the specific density and R_c is an in-house developed confidential variable correction factor which depends on local bathymetry in the hopper and on the suspended material in the current amongst other things. Erosion of the sediment bed occurs when the bed shear stress exceeds a threshold value based on the critical shields parameter.

There is also sediment entrainment between the internal current and the external current due to flow velocity differences. Sediment is transported into the current with the highest velocity. The sediment entrainment flux reads:

$$P_{E,\phi} = -\alpha_e \rho_s \phi_k \left|\frac{\Delta U}{U}\right| \cdot \Delta U$$

(12)

Where ϕ_k is the cross-section averaged concentration of fraction k of either the internal or external current depending on the sign of the entrainment flux, ΔU is the relative velocity difference between the two currents and α_e is a confidential entrainment coefficient.

The bed shear stress τ_b is defined as:

$$\tau_b = \rho_m c_D U^2$$

(13)

The model simulates transport of water and sediment inside a hopper with cross section averaged conservation equations of mass and momentum.

Where ρ_m is the density of the overlaying current, U is the flow velocity of the overlaying current and c_D is a constant drag coefficient. Interfacial friction is neglected because a sensitivity analyses showed minor differences when included.

Numerical integration scheme

The full set of conservation equations for both the external and internal current are discretised as follows:

$$\frac{\partial \boldsymbol{V}}{\partial t} + \frac{\partial \boldsymbol{F}}{\partial x} = \boldsymbol{S}$$

(14)

Where V is the vector of conserved variables, F is the flux vector and S is the source/sink vector (see 14-1).

The system of equations shown in (14-1) is solved on a staggered grid (see Figure 4) where j is a spatial node and δx is a spatial step.

Finite volume upwind scheme

The system shown in Figure 4 has been discretised based on the finite volume space discretisation with upwind schemes for the fluxes on a staggered grid and with a time explicit scheme. Upwind discretisation is used because of its robustness, simplicity and relative low computational effort. The discretisation is first order accurate and its linear stability condition is expressed with the courant number (Hirsch, 2007).

Momentum balance of the external current model

The momentum balance for positive flow

$$\left(\frac{U^n_{j-1/2}+U^n_{j+1/2}}{2} > 0,\ \frac{U^n_{j-3/2}+U^n_{j-1/2}}{2} > 0\right)$$

reads: (see 15)

The momentum balance for negative flow

$$\left(\frac{U^n_{j-1/2}+U^n_{j+1/2}}{2} \le 0,\ \frac{U^n_{j-3/2}+U^n_{j-1/2}}{2} \le 0\right)$$

reads:(see 16)

Mass balance of the external current model

The mass balance for positive flow

$$(U^n_{j+1/2} > 0,\ U^n_{j-1/2} > 0)$$

reads:

$$\frac{A^{n+1}_j - A^n_j}{\Delta t} + \frac{\left(U^n_{j+1/2}A^n_j - U^n_{j-1/2}A^n_{j-1}\right)}{\Delta x} = S^n_j$$

(17)

The mass balance for negative flow

$$(U^n_{j+1/2} \le 0,\ U^n_{j-1/2} \le 0)$$

reads:

$$\frac{A^{n+1}_j - A^n_j}{\Delta t} + \frac{\left(U^n_{j+1/2}A^n_{j+1} - U^n_{j-1/2}A^n_j\right)}{\Delta x} = S^n_j$$

(18)

Where the source/sink terms S^n_j are straightforward to discretise.

Suspended-sediment concentration balance of the external current model

The suspended sediment concentration balance for positive flow

$$(U^n_{j+1/2} > 0,\ U^n_{j-1/2} > 0)$$

reads:

$$\frac{(\phi A)^{n+1}_j - (\phi A)^n_j}{\Delta t} + \frac{\left(U^n_{j+1/2}(\phi A)^n_j - U^n_{j-1/2}(\phi A)^n_{j-1}\right)}{\Delta x} = S^n_j$$

(19)

The suspended sediment concentration balance for negative flow

$$(U^n_{j+1/2} \le 0,\ U^n_{j-1/2} \le 0)$$

reads:

$$\frac{(\phi A)^{n+1}_j - (\phi A)^n_j}{\Delta t} + \frac{\left(U^n_{j+1/2}(\phi A)^n_{j+1} - U^n_{j-1/2}(\phi A)^n_j\right)}{\Delta x} = S^n_j$$

(20)

Momentum, mass and suspended sediment balance of the internal current model

The momentum balance for positive flow reads: (see 21)

The momentum balance for negative flow reads: (see 22)

The mass and suspended sediment balances of the internal current model are analogues to the discretisation of the mass and suspended sediment balances of the external current model except for the source/sink terms.

Model assessment

In this chapter the discretisation of specific parts of both model equations are extensively tested for conservation of mass, momentum and mechanical energy against analytical solutions for the following idealised cases:

$$V = \begin{bmatrix} A_e \\ \phi_e A_e \\ A_e U_e \\ A_i \\ \phi_i A_i \\ A_i U_i \end{bmatrix}, \quad F = \begin{bmatrix} A_e U_e \\ \phi_e A_e U_e \\ A_e (U_e)^2 \\ A_i U_i \\ \phi_i A_i U_i \\ A_i (U_i)^2 + \frac{1}{2}\varepsilon g h A_i \end{bmatrix},$$

$$S = \begin{bmatrix} -\frac{\rho_b}{\rho_w}\frac{\partial A_b}{\partial t} + \left(P_{in,w,e} + P_{in,\phi,e}\right)B/\rho_w - \Delta\left(\left(P_{in,\phi,e}B + (E-D)B - P_{ov,\phi}B_{ov}\right)/\rho_s\right) - \left(P_{ov,w} + P_{ov,\phi}\right)B_{ov}/\rho_w \\ \left(P_{in,\phi,e}B + (E-D_e)B + P_{E,\phi}B + P_{upw,\phi}B - P_{ov,\phi}B_{ov}\right)/\rho_s \\ -gA_e\frac{\partial \xi_e}{\partial x} - c_f|U_e|U_e P \\ -\frac{\rho_b}{\rho_w}\frac{\partial A_b}{\partial t} - \Delta\left(\left(P_{in,\phi,i}B + D_e B + (E-D_i)B - P_{E,\phi}B - P_{upw,\phi}B\right)/\rho_s\right) + \left(P_{in,\phi,i} + P_{in,w,i}\right)B/\rho_w \\ \left(P_{in,\phi,i}B + D_e B + (E-D_i)B - P_{E,\phi}B - P_{upw,\phi}B\right)/\rho_s \\ -\frac{\rho_e}{\rho_i}gA_i\frac{\partial \xi_e}{\partial x} - \varepsilon g A_i\frac{\partial z}{\partial x} - \frac{\tau_b B_b}{\rho_i} - \frac{U}{\sqrt{U^2}}\frac{\tau_i B_i}{\rho_i} \end{bmatrix}$$

(14-1)

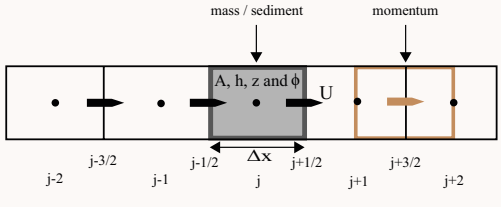

FIGURE 4

Schematisation of the staggered grid approach.

$$\frac{U_{j-1/2}^{n+1}A_{j-1/2}^{n}-(UA)_{j-1/2}^{n}}{\Delta t}+\frac{\left(U_{j}^{n}(UA)_{j-1/2}^{n}-U_{j-1}^{n}(UA)_{j-3/2}^{n}\right)}{\Delta x}+gA_{j-1/2}^{n+1}\frac{\left(\xi_{j}^{n+1}-\xi_{j-1}^{n+1}\right)}{\Delta x}$$
$$=-c_f U_{j-1/2}^{n}\left|U_{j-1/2}^{n}\right|P_{j-1/2}^{n}$$

(15)

$$\frac{U_{j-1/2}^{n+1}A_{j-1/2}^{n}-(UA)_{j-1/2}^{n}}{\Delta t}+\frac{\left(U_{j}^{n}(UA)_{j+1/2}^{n}-U_{j-1}^{n}(UA)_{j-1/2}^{n}\right)}{\Delta x}+gA_{j-1/2}^{n+1}\frac{\left(\xi_{j}^{n+1}-\xi_{j-1}^{n+1}\right)}{\Delta x}$$
$$=-c_f U_{j-1/2}^{n}\left|U_{j-1/2}^{n}\right|P_{j-1/2}^{n}$$

(16)

$$\frac{\frac{1}{2}U_{j-1/2}^{n+1}\left(A_{j-1/2}^{n+1}+A_{j-1/2}^{n}\right)-(UA)_{j-1/2}^{n}}{\Delta t}+\frac{\left(U_{j}^{n}(UA)_{j-1/2}^{n}-U_{j-1}^{n}(UA)_{j-3/2}^{n}\right)}{\Delta x}+\frac{1}{2}g\frac{\left(\varepsilon_{j}^{n}h_{j}^{n}A_{j}^{n}-\varepsilon_{j-1}^{n}h_{j-1}^{n}A_{j-1}^{n}\right)}{\Delta x}$$
$$+\frac{1}{2}\frac{\rho_e}{\rho_i}gA_{j-1/2}^{n}\frac{\left(\xi_{j}^{n}-\xi_{j-1}^{n}\right)}{\Delta x}+\varepsilon_{j-1/2}^{n}gA_{j-1/2}^{n}\frac{\left(z_{j}^{n}-z_{j-1}^{n}\right)}{\Delta x}=-c_D U_{j-1/2}^{n}\left|U_{j-1/2}^{n}\right|P_{j-1/2}^{n}$$

(21)

$$\frac{\frac{1}{2}U_{j-1/2}^{n+1}\left(A_{j-1/2}^{n+1}+A_{j-1/2}^{n}\right)-(UA)_{j-1/2}^{n}}{\Delta t}+\frac{\left(U_{j}^{n}(UA)_{j+1/2}^{n}-U_{j-1}^{n}(UA)_{j-1/2}^{n}\right)}{\Delta x}$$
$$+\frac{1}{2}g\frac{\left(\varepsilon_{j}^{n}h_{j}^{n}A_{j}^{n}-\varepsilon_{j-1}^{n}h_{j-1}^{n}A_{j-1}^{n}\right)}{\Delta x}+\frac{1}{2}\frac{\rho_e}{\rho_i}gA_{j-1/2}^{n}\frac{\left(\xi_{j}^{n}-\xi_{j-1}^{n}\right)}{\Delta x}$$
$$+\varepsilon_{j-1/2}^{n}gA_{j-1/2}^{n}\frac{\left(z_{j}^{n}-z_{j-1}^{n}\right)}{\Delta x}=-c_D U_{j-1/2}^{n}\left|U_{j-1/2}^{n}\right|P_{j-1/2}^{n}$$

(22)

- the dam break,
- transitions from subcritical flow to supercritical flow and vice versa,
- the horizontal transport and sedimentation
- the lock exchange.

Dam break case

Stoker (1957) examined dam break problems analytically. He derived expressions for horizontal propagating free-surface fronts at frictionless conditions. These analytical expressions allow us to test parts of the external model for mass and momentum conservation and flooding and drying of the sediment bed.

First a wet bed dam break case is considered. After release of the dam two fronts starts to propagate in upstream and downstream direction. The simulated water level and velocity show accurate agreement with the analytical solutions (see Figure 5).

The simulated results show smooth transitions near steep gradients due to numerical (artificial) diffusion from the upwind scheme (Hirsch, 2007). It can be suppressed to a certain degree by reducing the spatial step.

Next, a dry bed dam break case is simulated (see Figure 6). After release of the dam two fronts start to propagate in opposite direction (see Figure 6A).

The simulated water levels and velocities show satisfactory agreement with the analytical solution apart from a small area near the front at very small layer height. However, simplifying assumptions to derive the analytical solutions and highly non-linear effects preclude an exact comparison of simulated and analytical results near the front at very small layer height O (0.5mm).

Transitions from subcritical flow to supercritical flow and vice versa

Here, the external current model for incompressible frictionless steady state flows over a continuous bed profile is tested to examine conservation of mass and mechanical energy. The analytical solution can be derived from Euler's one-dimensional non-viscous equation of motion with assumptions of steady state and incompressible flow. Then, the conservation of mechanical energy along a streamline (Bernoulli) reads:

$$\frac{\partial}{\partial x}\left(\frac{1}{2}u^2+\frac{p}{\rho}+gz\right)=0$$

(23)

First, a steady state transition from a subcritical flow to a supercritical flow over a continuous smooth bed profile is considered. The simulated water level profile and discharge

FIGURE 5

Simulation of a dam break case. The dam is located at x = 1000 m. and the initial water levels at the upstream and downstream side of the dam are 1.0 m and 0.1 m, respectively (Δx = 1.0 m, Δt = 0.025 s). Graph (A) and (B) show the analytical (black) and simulated (blue) water level and the horizontal layer average velocity along the domain after 300 s, respectively.

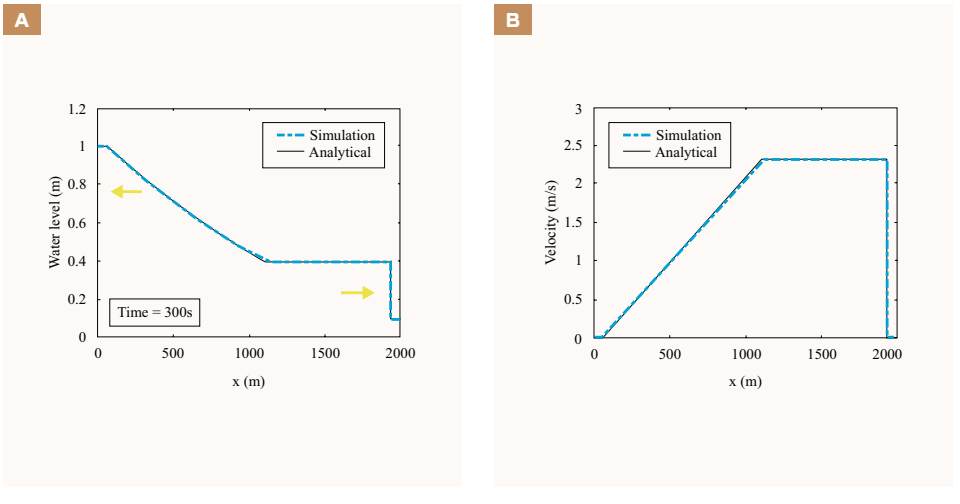

A

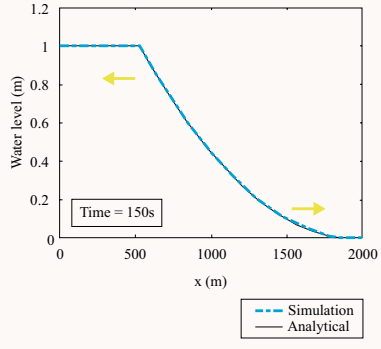

B

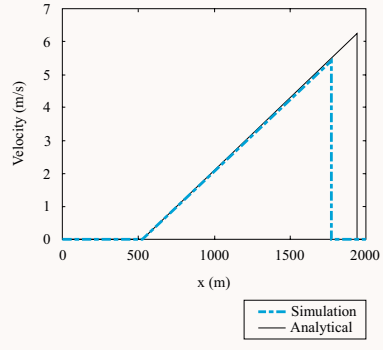

FIGURE 6

Simulation of a dam break case. The dam is located at x = 1000 m with a water level at the upstream side of 1.0 m and a dry bed at the downstream side (Δx = 1.0 m, Δt = 0.025 s). Graph (A) and (B) show the analytical (black) and simulated (blue) water level and horizontal layer average velocity along the domain after 150 s, respectively.

show accurate agreement with the analytical solution (see Figure 7).

This indicates conservation of mass and mechanical energy. Moreover, the model can deal with a transition from subcritical flow to supercritical flow.
Next to consider are steady state hydraulic jumps over a horizontal bed to examine the transitions from supercritical flow to subcritical flow based on Bélanger's equation derived from mass and momentum conservation (1841):

$$\frac{H_2}{H_1} = \frac{1}{2}\left[(1 + 8Fr_1^2)^{1/2} - 1\right]$$

(24)

Where Fr_1 is the Froude number at the upstream side of the hydraulic jump and H_1 and H_2 are the water depths at the upstream and downstream side, respectively.
The accurate agreement of the simulated ratios downstream to upstream water depth for different Froude numbers with the analytical solution (see Figure 8C) demonstrates that the model can deal with transitions from supercritical flow to subcritical flow.

Horizontal transport and sedimentation case

The model for proper transport of suspended sediment by horizontal advection and settling is tested. To that end, the model is verified against an analytical expression for the horizontal sediment concentration distribution derived from the 1DH transport equation with the assumptions of steady state, constant discharge, constant inflow sediment concentration, constant width and constant settling velocity. The analytical solution for the horizontal sediment concentration distribution reads:

$$\frac{\phi}{\phi_0} = \exp\left(-\frac{x}{L_{sed}}\right), \quad with\ L_{sed} = \frac{q}{w_s}$$

(25)

Where ϕ is the suspended concentration, ϕ_o is a constant inflow concentration at the upstream boundary, q is the constant discharge per unit width at the upstream boundary, w_s is a constant settling velocity, x is the spatial distance from the upstream boundary and L_{sed} is the sedimentation length.

The numerical solutions converge with increasing number of grid cells towards the analytical solutions (see Figure 9). At low spatial resolution the first order upwind discretisation causes longitudinal numerical diffusion resulting in an over prediction of the length scale over which sediment settles

A

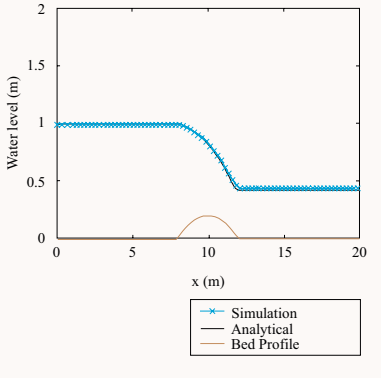

B

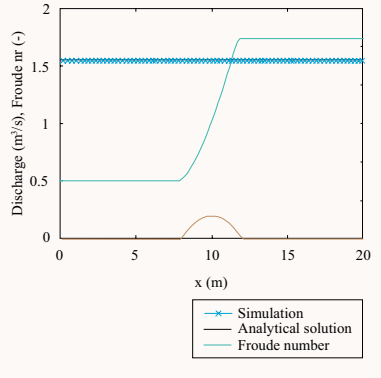

FIGURE 7

Steady state simulation of the transition from subcritical flow to supercritical flow over a continuous bed profile with an upstream discharge of 1.55 m3/s (Δx = 0.5 m, Δt = 0.025 s). Graph (A) and (B) show the analytical (black) and simulated (blue) water levels, discharges and Froude number (green) along the domain, respectively.

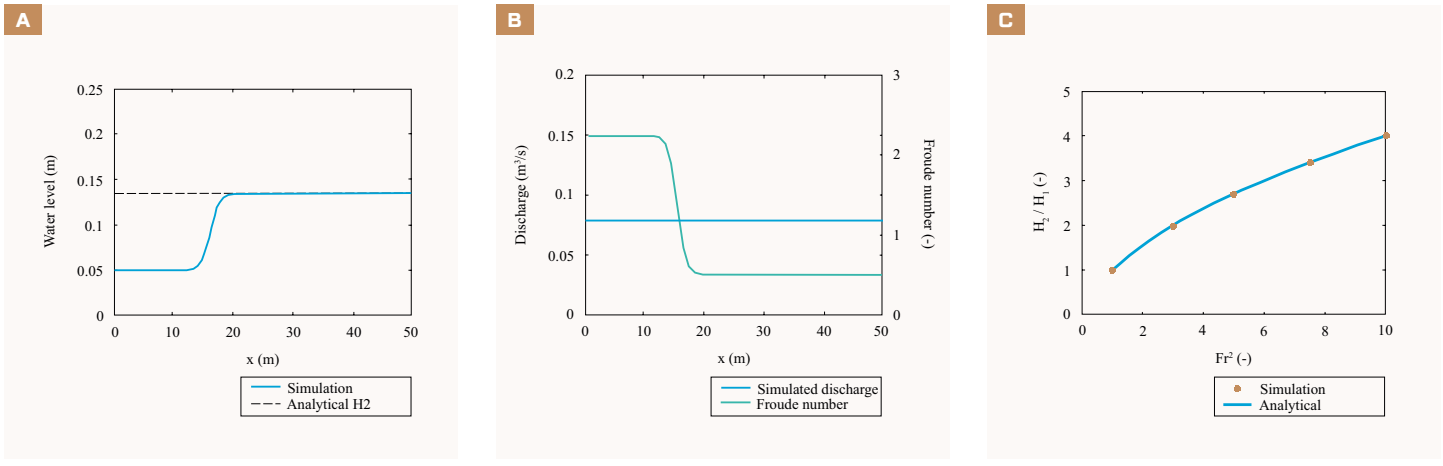

FIGURE 8

Steady state hydraulic jump simulations with an upstream Froude number of Fr_1^2 = 5 and a downstream water depth of 0.13 m at x = 500 m (Δx = 1.0 m, Δt = 0.025 s) (Graphs a and b). Graph (A) and (B) show the analytical (black) downstream water depth and the simulated (blue) water depth and discharge along the domain, respectively. Graph (C) shows simulated (red dots) and analytical (blue line) ratios of the downstream (x = 40 m) to upstream water depth (x =10 m) for steady state hydraulic jump simulations at different upstream Froude numbers.

(N=25). However, by increasing the resolution through the application of more grid cells (N=100), the numerical diffusion can be suppressed such that the numerical results show accurate agreement with the analytical solution.

Lock-exchange case

The dynamical progression of an axis-symmetric gravity current is examined to verify whether the model properly simulates baroclinic currents. Their proper simulation hinges on mass and momentum conservation as well as adequate reproduction of baroclinic gradients. The simulated propagation distance of an axis-symmetric gravity current with time is tested against semi-empirical relations from Hallworth et al. (1996) in de Nijs (2010).

In the model, a gravity current starts to propagate along the bed after the release of a block of dense fluid within a fluid of low density (see Figure 10A, B).

In the model there is some transition period before the block of dense fluid evolves into a gravity current (de Nijs, 2010). After this transition period, the simulated distance travelled by the head of the gravity current shows accurate agreement with the analytical solutions (see Figure 10C).

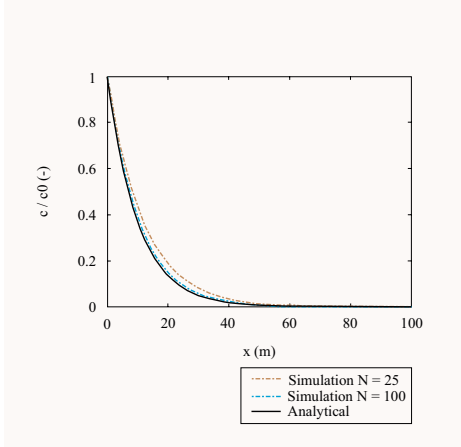

FIGURE 9

Simulation of horizontal transport and sedimentation along a domain of 100 m with a constant discharge per unit width of q = 10 m²/s, a constant inflow concentration of ϕ = 0.2 [-] and a constant settling velocity of 1.0 m/s (Δx = 4.0 m, Δt = 0.2 s and Δx = 1.0 m, Δt=0.05 s). The figure shows the analytical (black) and simulated (red and blue) normalised concentration profiles for 25 and 100 grid cells after 50s.

Model validation

The external and internal current models form the hopper sedimentation model. This model is validated for the total cumulative overflow losses with data from laboratory model tests and prototype measurements of TSHD Cornelia (van Rhee, 2002), and Van Oord's TSHD Vox Maxima and Volvox Atalanta. For the model calibration, the laboratory model Tests 5 and 6 (van Rhee, 2002) are used. For validation, an independent set of laboratory model Tests (7, 8, 9 and 12) and the prototype measurements are used to indicate the predictive capability and to exclude scale effects.

The modelled and measured total cumulative overflow losses show good one to one agreement (see Figure 11A). The goodness of fit of the model to measurements (see Figure 11A), based on the coefficient of determination , of 0.90 is favourably high. It is noted that a proper reproduction of the overflow losses required the specification of particle size distributions.

The simulated final along hopper sediment bed layer distribution of Vox Maxima shows good agreement with hopper soundings (see Figure 11B, C). These results are promising, but soundings over a wider range of

conditions are required to validate the model's bed level elevation predictions.

Conclusions

The following conclusions can be drawn from verification and validation:

- The verification of specific parts of the numerical model to analytical solutions demonstrates that the model satisfactory simulates barotropic and baroclinic currents that require proper mass, momentum and mechanical energy conservation.
- Furthermore, the model can deal with drying and flooding of the sediment bed and with transitions from subcritical flow to super-critical flow and vice versa.
- The validation of the hopper sedimentation model to laboratory experiments and prototype measurements demonstrates that the model predicts the total cumulative overflow losses favourably well for a wide range of conditions and scales.

The model performs well even though several physical simplifications have been made. Therefore, for our purposes, we can assume that it includes the essential physics involved in hopper sedimentation for sufficient predictive power. Although the model predicts the total cumulative overflow losses well, future efforts are directed towards further validation to prototype data for overflow losses as well as for the along hopper sediment bed layer distribution. Preliminary results of the latter are promising (not all shown). We will also investigate whether the predictions improve by taking into account turbulent mixing.

Currently, we apply our model as a simulator to test working strategies and to develop and test dredging loading automation e.g. draught, water level and trim control by managing anti-pollution valves, overflow positions and inflow positions amongst other things. To this end we included the effect of the along hopper sediment bed layer distribution on ship draught and trim by coupling the model with vessel specific hydrostatic tables. We also use this simulation model in new build projects, for instance to determine the appropriate height of transverse hopper bulkheads.

The model performs with low computational effort: only a couple of minutes simulation time for prototype conditions on an ordinary PC.

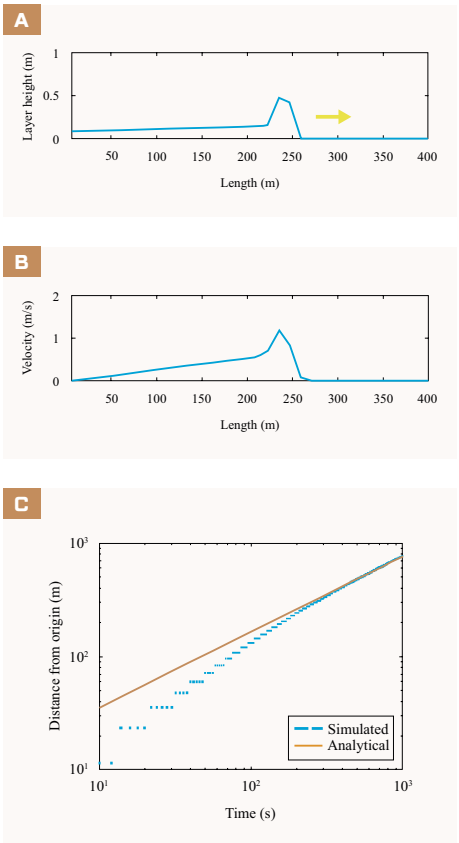

FIGURE 10

Simulation of an axis-symmetric gravity current with a concentration of the lock of 0.1 [-] , and a lock length and height of 25 m and 3.0 m, respectively (Δx = 5.0 m, Δt = 0.5 s). The settling velocity is set naught. Graph (A) and (B) show the simulated height of the gravity current and the horizontal layer averaged velocity along the domain after 200 s, respectively. Graph (C) shows the simulated (blue) and analytical (red) distance travelled by the gravity current from the origin vs time on a log-log scale.

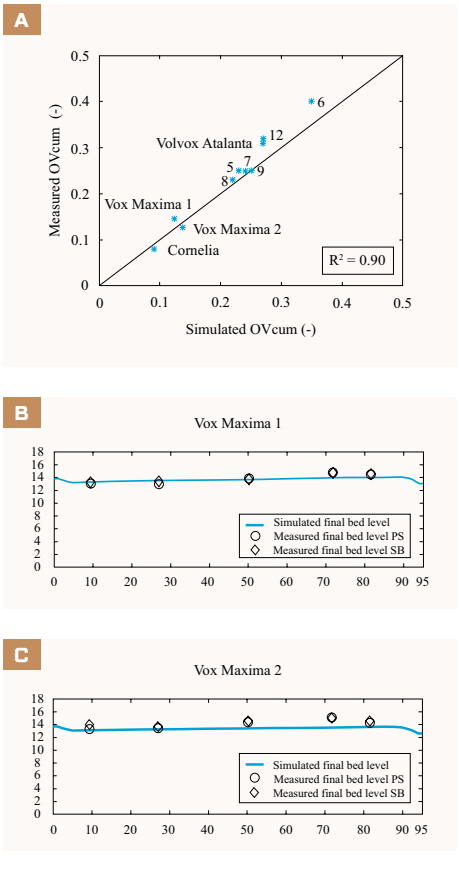

FIGURE 11

Graph (A) show the one to one comparison of measured total cumulative overflow losses versus simulated total cumulative overflow losses for a wide range of conditions. The R^2 coefficient is 0.90. The operational parameters, particle size distributions and the hopper geometry for both the laboratory model tests and the prototype test of TSHD Cornelia can be found in Van Rhee (2002). Graph (B) and (C) show the final along hopper sediment bed layer distribution of TSHD Vox Maxima.

Summary

This article describes the development, verification and validation of a new transient one-dimensional cross-sectional averaged numerical model to predict the sedimentation process inside hoppers of TSHDs. The model includes an external current model and an internal current model both based on cross-section averaged equations for mass and momentum in conservative forms to simulate barotropic and baroclinic flows.

First presented as a paper at the CEDA Dredging Days Conference 2017, this article has been published in a slightly adapted version with permission of the copyright holder, CEDA. At the conclusion of the conference, IADC's Secretary General René Kolman bestowed the Young Author Award to Jordy Boone to recognise his outstanding paper and presentation.

Jordy Boone
After obtaining his bachelor's degree in Marine Technology from Delft University of Technology, Jordy acquired an MSc degree in Offshore and Dredging Engineering from the university in 2016. After graduating, he joined Van Oord Dredging and Marine contractors as a Dredging Research and Development Engineer. Within Van Oord, he is involved in the research of hopper sedimentation processes and hopper loading strategies.

Michel A.J. de Nijs
Michel earned his BSc and MSc degrees in Civil Engineering (Cum Laude) and PhD degree in estuarine oceanography from Delft University of Technology. As a team leader Dredging Research & Development at Van Oord, he provides expertise in dredging projects with emphasis on fluid mechanical, geotechnical, geomechanical and mechanical aspects related to new build/modification of equipment, working strategies, automation and dredging construction project support.

REFERENCES

Camp, T. (1946)
Sedimentation and the design of settling tanks. Trans. ASCE, 895-936.

Ferguson, R., & Church, N. (2004)
A simple universal equation for grain settling velocity. Journal of sedimentary research , 933-937.

Hallworth, M., Huppert, H., Phillips, J., & Sparks, R. (1996)
Entrainment into two-dimensional and axisymmetric turbulent gravity currents. Journal of Fluid Mechanics, 208, 289-311.

Hirsch, C. (2007)
Numerical computation of internal and external flows. Oxford: John Wiley & Sons.

Koning , J. de (1977)
Constant loading system of trailing suction hopper dredgers. Proc. Int. Course on modern dredging, Den Haag .

Miedema, S.A., & Vlasblom, W.J. (1996)
Theory for hopper sedimentation. 29th Annual Texas A&M Dredging Seminar. New Orleans.

Nijs, M. A. J. de (2010)
The 2DH modelling of turbidity currents generated by water injection dredging. Wodcon 2010.

Nijs, M. A. J. de, Pietrzak, J.D., & Winterwerp, J.C. (2011)
Advection of the Salt Wedge and Evolution of the Internal Flow Structure in the Rotterdam Waterway. Journal of Physical Oceanography, 41, 3–27.

Richardson, J.F., & Zaki, W.N. (1954)
Sedimentation and fluidization: I. Trans. Inst. Chem. Eng., 32(35):112.

Rhee, P. C. van (2002)
On the sedimentation process in a trailing suction hopper dredger. PhD thesis, Delft University of Technology.

Rijn, L. van (1984)
Sediment Pick-up Functions. J. Hydr. Eng. ASCE, 110(10): 1494-1502.

Rowe, P.N. (1987)
A convenient empirical equation for estimation of the Richardson-Zaki exponent. Chem. Eng. Science, 2795-2796.

Spearman, J. (2014)
Prediction of the overflow of sediment from trailer dredgers . Maritime Engineering Volume 167, 82-96.

Stoker, J. J. (1957)
Water Waves, The mathematical theory with applications. Interscience Publishers.

Vlasblom, W., & Miedema, S. (1995)
A Theory for determining sedimentation and overflow losses in hoppers. Amsterdam: 14th World Dredging Congress.